Table III. Thermodynamic Quantities of Transfer from Organic to Water Phase at 30 °C

solute	organic solvent	ΔG_{tr}, cal mol^{-1}	ΔH_{tr}, cal mol^{-1}	ΔS_{tr}, cal mol^{-1} deg^{-1}
1-naphthol	cyclohexane	-4808.00	2942.00	-27.10
2-naphthol	cyclohexane	-5268.00	2590.00	-24.43
1-naphthol	benzene	-47751.00		
2-naphthol	benzene	-47740.00		

K_s values are consistently lower.

The three thermodynamic parameters of transfer for the naphthols are recorded in Table II. The values show that the free energies of transfer for the naphthols at all temperatures are positive for all salts except KSCN which shows negative values. Also ΔG_{tr} values at a particular temperature and for a particular salt are higher in 1-naphthol than in 2-naphthol. With the increase in temperature the ΔG_{tr} values decrease, the effect being pronounced between 20 and 30 °C.

During salting-out, salts are solvated with water molecules thus decreasing the availability of water for the nonelectrolyte. As a result the free energy for the latter rises thereby showing positive ΔG_{tr} values. The reverse phenomenon occurs in the case of KSCN, i.e., increasing the solubility of the nonelectrolyte in KSCN solutions thereby resulting in salting-in.

The ΔH_{tr} values are negative in all cases except in the case of KSCN. An exothermic ΔH_{tr} value indicates a net structure breaker and an endothermic value indicates a net structure maker. The exothermic ΔH_{tr} values are highest in the case of studies with Na_2SO_4 followed by NaCl, $NaClO_4$, and endothermic in case of KSCN. When the naphthols enter salt solution, where the salt is KSCN, heat is required to accommodate the naphthol molecules, thereby showing the structure-making tendency of KSCN, solute–water or solute–salt interaction being negligibly small.

The ΔS_{tr} values are found to be small and negative in case of studies with all salts except KSCN where positive values are obtained. Thus we can say when the naphthols are transferred from water to salt solutions, the forces on the neighboring water molecules are modified, decreasing the net entropy. As the ΔS_{tr} values are small it is logical to state that in the presence of ionic fields, the naphthols have relatively little influence on the solvent molecules. The small values of entropy also indicate that for a particular transfer process, entropy is only a secondary driving force. Table III shows the thermodynamic quantities of transfer from the organic to the water phase. Here we obtain free energies of transfer which are negative in contrast to those obtained in case of transfer from water to salt solutions. The free energy of nonelectrolyte in organic solvents are expected to be higher than in water solutions. Interestingly, these values for the naphthols with benzene in the organic phase are much lower than when benzene is replaced by cyclohexane. A plausible explanation of this behavior undoubtedly lies in the fact that in benzene solutions, strong $\pi-\pi$ interactions operate which is absent in cyclohexane (*8*). This may be a major factor contributing to the observed difference in ΔG_{tr} in the two cases reported in Table III.

Acknowledgment

A part of the work was done by B.D.B. at Roorkee during her tenure in the Department of Chemistry, University of Roorkee, U.P., as a Senior C.S.I.R. research fellow.

Registry No. NaCl, 7647-14-5; Na_2SO_4, 7757-82-6; $NaClO_4$, 7601-89-0; KSCN, 333-20-0; 1-naphthol, 90-15-3; 2-naphthol, 135-19-3; cyclohexane, 110-82-7; benzene, 71-43-2.

Literature Cited

(1) Ghosh, R.; Das, B. *J. Indian Chem. Soc.* **1981**, *58*, 1108.
(2) Korenman, I. M. "Ekstraktsiya V Analize Organicheskikh Veshchestv" (Extraction in the Analysis of Organic Compounds); Khimiya; Moscow, 1977; p 43.
(3) Das, B.; Ghosh, R. *J. Chem. Eng. Data* **1983**, *28*, 45.
(4) Das, B.; Ghosh, R. *J. Chem. Eng. Data* **1984**, *29*, 137.
(5) Setschenow, J. *Z. Phys. Chem.* **1889**, *4*, 117.
(6) Long, F. A.; McDevit, W. F. *Chem. Rev.* **1952**, *51*, 119.
(7) Franks, F. "Water"; Plenum Press: New York, 1972; Vol. 1.
(8) Tanford, C. "The Hydrophobic Effect"; Wiley-Interscience: New York, 1973; p 8.

Received for review December 26, 1984. Accepted May 28, 1985. Thanks are due to the UGC, New Delhi, for the award of a Research Associateship.

Diffusion, Viscosity, and Refractivity Data on the System Dimethylformamide–Water at 20 and 40 °C

Claudio Della Volpe, Gennaro Guarino, Roberto Sartorio, and Vincenzo Vitagliano*

Dipartimento di Chimica, Università di Napoli, 4 Via Mezzocannone, Naples, Italy

The diffusion coefficients of the system dimethylformamide–water at 20 and 40 °C were measured in all the ranges of concentration by the Gouy technique. In the same ranges viscosities and densities were also measured. From these data the activation energies for diffusion and viscosity have been calculated. From diffusion data molar refractivities were obtained. It was confirmed that dimethylformamide and water have a strong interaction. We suggest that this interaction does not have the character of complex formation but rather that of an extended, clusterlike structure where the H bonds play a relevant role.

Introduction

In a previous article (*1*) the diffusive properties of *N*,*N*-dimethylformamide (DMF) at 5 °C were examined. In the present article we report diffusion data collected at 20 and 40 °C.

The interest of these data comes from the use of DMF as a solvent for the polymeric material used in membrane casting with the technique of "phase inversion" (*2*, *3*).

Notwithstanding the mechanism of membrane formation is not readily explicable, the solvent/nonsolvent interdiffusion process is certainly important (*4*–*6*). Water is generally the nonsolvent used with DMF. There is a lack of accurate diffusion data (*7*) for the DMF–H_2O system. For this reason we have collected the diffusion data through all the composition range and in a wide temperature interval.

Density, refractivity, and viscosity data have also been collected at the same temperatures.

Experimental Section

Material. Dimethylformamide, reagent grade (C. Erba, Milan and Baker Chemicals, Holland), was used without further pu-

0021-9568/86/1731-0037$01.50/0

Table I. Diffusion Data[a]

X_1	ΔX_1	J_m	10^5D	ΔC_1
	a. DMF–H_2O at 20 °C			
0			(1.011)	
0.002575	0.00515	110.90	1.011	0.2809
0.0501	0.0049	83.90	0.885	0.2045
0.1430	0.0099	109.50	0.825	0.2664
0.2856	0.0133	72.60	0.821	0.2038
0.3980	0.0372	115.40	0.886	0.3865
0.6124	0.1033	121.70	1.040	0.5922
0.7201	0.1071	85.50	1.158	0.4769
0.8192	0.0774	38.05	1.321	0.2730
0.9592	0.0583	21.20	1.622	0.1670
1			(1.719)	
	b. DMF–H_2O at 40 °C			
0			(1.807)	
0.05013	0.0043	63.00	1.653	0.1771
0.1525	0.0087	84.50	1.488	0.2197
0.2884	0.0249	114.90	1.390	0.3677
0.4007	0.0310	87.00	1.419	0.3110
0.5064	0.0515	86.50	1.482	0.3765
0.6135	0.0967	107.00	1.560	0.5374
0.7173	0.1120	82.30	1.728	0.4884
0.7982	0.0767	40.80	1.950	0.2769
0.8994	0.0816	31.90	2.381	0.2378
0.9581	0.0646	20.80	2.751	0.1764
1			(3.081)	

[a] X_1 = mole fraction of DMF; ΔX_1 = mole fraction difference from upper and lower solution of each run; J_m = number of Gouy fringes; D = diffusion coefficient in $cm^2\ s^{-1}$; ΔC_1 = concentration difference from upper and lower solution of each run. ΔC_1 values were obtained from mole fractions by using the equation for density given in Table III.

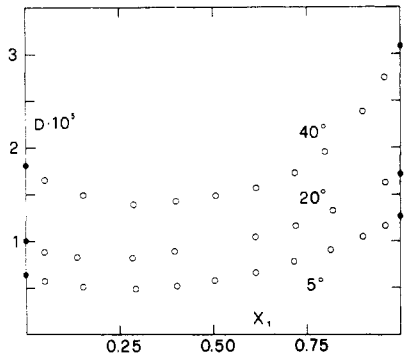

Figure 1. Diffusion coefficients (D in $cm^2\ s^{-1}$) of the system DMF–H_2O at various temperatures as a function of DMF mole fraction. Limiting values at $x_1 = 0$ are from the equations given in Table III. Data at 5 °C are from ref *1*.

rification. Solutions for all measurements were prepared by weighing both solute and solvent.

Diffusion runs were taken at 20 and 40 °C (±0.02 °C) by using the Gouy interferometric technique (*8*).

The experimental results are presented in Table I, parts a and b. Figure 1 is a graph of the diffusion coefficients vs. solute mole fraction for both temperatures.

Densities of solutions were measured with a A. Parr densitometer at 20 and 40 °C.

Viscosities were measured with an Ubbelohde viscosimeter (water flow times 127.6 s, at 20 °C and 79.4 s at 40 °C). Density and viscosity data are presented in Table II, a and b. Figures 2 and 3 show the graphs of density and viscosity.

Refractive Indexes of solutions were computed by integration of the function $\Delta n(c)$ between 0 and c, which represents the refractive index difference between top and bottom solutions of each diffusion run.

$\Delta n(c)$ was calculated by using the equation

$$\Delta n = J_m(\lambda/a) \qquad (1)$$

Table II. Density and Viscosity Data[a]

X_1	t/t^0	η, cP	X_1	d, g/cm³
		a. DMF–H_2O at 20 °C		
0.0000	1.000	1.002	0.0000	0.998 202
0.0217	1.223	1.2254	0.002797	0.998 054
0.0466	1.480	1.4830	0.005377	0.997 954
0.0989	2.007	2.0110	0.014765	0.997 812
0.1478	2.352	2.3567	0.028125	0.997 812
0.1960	2.645	2.6503	0.0765	0.999 156
0.2481	2.882	2.8878	0.1108	1.000 009
0.2859	2.902	2.9078	0.1457	1.000 415
0.3728	2.702	2.7074	0.1813	1.000 271
0.4919	2.257	2.2615	0.2007	0.999 841
0.5936	1.745	1.7485	0.2467	0.998 256
0.6889	1.434	1.4369	0.2958	0.995 753
0.7991	1.182	1.1844	0.3888	0.989 183
0.8795	1.071	1.0731	0.4890	0.981 526
1.0000	0.923	0.9248	0.6097	0.972 256
			0.6863	0.966 670
			0.7842	0.960 226
			0.8807	0.954 636
			1.0000	0.948 680
		b. DMF–H_2O at 40 °C		
0.0000	1.000	0.6529		0.992 214
0.0217	1.185	0.7737		0.990 477
0.0466	1.395	0.9108		0.989 193
0.0989	1.819	1.1876		0.987 510
0.1478	2.150	1.4037		0.986 107
0.1960	2.386	1.5578		0.984 062
0.2481	2.623	1.7126		0.981 164
0.2859	2.648	1.7289		0.978 692
0.3728	2.430	1.5865		0.971 866
0.4919	2.069	1.3509		0.962 324
0.5936	1.803	1.1772		0.953 838
0.6889	1.539	1.0048		0.947 435
0.7991	1.343	0.8768		0.940 222
0.8795	1.240	0.8096		0.935 601
1.0000	1.094	0.7143		0.929 435

[a] X_1 = mole fraction of DMF; d = density; t = flow time in s; t^0 = flow time of water; η = viscosity of solution.

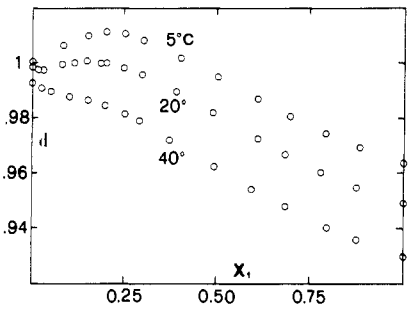

Figure 2. Densities (d in g/mL) of the system DMF–H_2O at various temperatures as a function of DMF mole fraction. Data at 5 °C are from ref *1*.

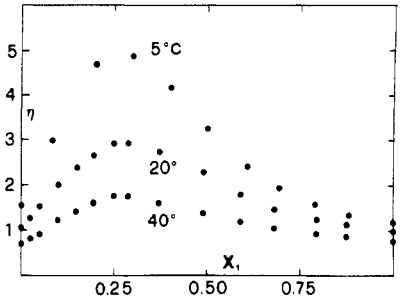

Figure 3. Viscosities (η in cP) of the system DMF–H_2O at various temperatures as a function of DMF mole fraction. Data at 5 °C are from ref *1*.

Table III. Coefficients of the Equation $Z = A_0 + A_1y + A_2y^2 + ... + A_Ny^N \pm E$

Z	10^5D^a	d	J_m/C_1	$n_{Hg}{}^b$	$R_m{}^c$	η,^{d} cP	R_m
y	X_1	X_1	C_1	C_1	X_1	X_1	X_1
			System DMF (1)–H_2O (2) at 20 °C				
A_0	1.011	0.99812	391.7	1.33447	3.703	1.003	3.729
A_1	−2.816	-9.166×10^{-4}	11.85	8.539×10^{-3}	16.286	9.652	16.205
A_2	13.05	3.563×10^{-1}	−0.8135	1.291×10^{-4}		17.49	0.0906
A_3	−25.12	−2.326	−0.1370	-5.912×10^{-6}		−172.4	
A_4	23.52	4.606		-7.468×10^{-7}		322.1	
A_5	−7.927	−3.929				−244.6	
A_6		1.245				67.61	
E	0.008	0.0026	5		0.008	0.017	0.003
			System DMF (1)–H_2O (2) at 40 °C				
A_0	1.807	0.99219	290.2	1.33204	3.696	0.6539	3.713
A_1	−3.504	−0.07781	38.41	6.328×10^{-3}	16.10	4.668	15.96
A_2	10.81	0.4958	−4.130	4.158×10^{-4}		18.89	0.1478
A_3	−14.63	−2.300		-3.002×10^{-5}		−139.9	
A_4	8.600	4.207				274.6	
A_5		−3.458				−228.3	
A_6		1.070				70.14	
E	0.007	0.0001	5		0.013	0.014	0.005

$^a D$ = diffusion coefficient in $cm^2\ s^{-1}$. $^b n$ = refractive index at the wavelength of Hg green light (546.07 nm). $^c R_m$ = molar refractivity (eq 2). $^d \eta$ = viscosity in cP.

where a (=2.500 cm) is the diffusion cell thickness, λ the Hg green line wavelength (λ = 546.1 nm), and J_m the Gouy fringe number.

The refractive indices of water at 20 and 40 °C were computed from the data given in ref 9: $n^{20}_{Hg} = 1.33447$; $n^{40}_{Hg} = 1.33204$; (this last value has been graphically interpolated by data of n vs. λ).

This result is coincident, within the experimental error, with that obtained by using the equation of n vs. t reported in the same reference.

Molar refractivities were obtained by using the equation

$$R_m = \frac{n^2 - 1}{n^2 + 2}(X_1M_1 + X_2M_2)/d \qquad (2)$$

where X_1, M_1, X_2, M_2 are the mole fractions and molecular weights of solute and water, respectively, and d is the density.

Molar refractivity is almost a linear function of mole fraction for both systems. Table III gives the polynomial coefficients for R_m fitted both with a linear function and with a parabola. The parabolic function leads to a smaller standard deviation for the R_m data, suggesting the presence of a small excess refractivity; however, such an excess is almost within the experimental error and so we prefer not to speculate about it.

Activation energies for diffusion and viscosity were computed including also the data from the ref 1 and 7 at 5 and 25 °C; the results are represented in Figure 4.

They are obtained from the equations

$$\ln \eta = (E_v/RT) + \text{const} \qquad (3)$$

$$\ln (D/T) = (-E_d/RT) + \text{const} \qquad (4)$$

where E_v and E_d are the activation energies for viscosity and diffusion.

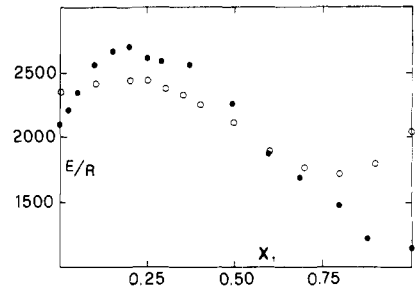

Figure 4. Activation energies for the diffusion (○) and viscous (●) processes from eq 3 and 4 for the system DMF–H_2O.

Discussion

Previously collected data (1), at 5 °C, and literature data (10–13) showed a peculiar trend of diffusion, viscosity, and density properties. Similar trends are visible also in present data.

Diffusion coefficients show a minimum at a DMF molar fraction about 0.25 corresponding at a H_2O/DMF ratio ca. 3.

There is a marked correspondence with viscosity data that show a maximum at the same composition.

On the other hand the density behavior does not show any well-defined extremum in this composition range. At low temperature a density maximum appears at a DMF mole fraction about 0.20–0.25 (1). By increasing temperature this maximum shifts to a lower DMF mole fraction and it disappears at 40 °C, being substituted by two inflection points (see Figure 2).

Molar refractivity is a linear function of molar fraction and, as at 5 °C, the second-order term is almost within the experimental error.

The obtined data confirm that in these solutions there is a significant interaction between water and DMF.

Two different interaction models have been suggested for the DMF–H_2O system:

(a) some strong, well-defined complexes of type DMF·$(H_2O)_n$ are present in solution and it has been generally assumed n = 3 (14–20);

(b) the DMF–H_2O interaction is due to the growth of extended, clusterlike structures where the H bonds play a relevant role (21–23).

In fact one must account for H bond on the *O*-carbonyl, H bond on the *N*-aminic, and the hydrophobic effect around DMF methyl group which promotes formation of water–water H bonds.

In our opinion the linear trend of molar refractivity can be an evidence in favor of model b.

The presence of extended H-bond structures in solution also explains the extrema observed both in the diffusion and viscosity behavior (Figure 1 and 3).

On the other hand the density data trend seems to be more sensitive to the water structure breaking due to the DMF addition, so that the density maximum is neither localized to any

particular mole fraction nor even well-defined; in fact it disappears at higher temperatures where the water structure is already partially destroyed.

It is interesting to note the different trend of the diffusion and viscosity activation energies. Both have a maximum at a DMF mole fraction ca. 0.2, which corresponds approximately to the composition range where a wider DMF–H_2O clusterlike structure can grow, according to model b.

At high DMF mole fraction, the diffusion activation energy exhibits also a minimum, which is absent in the viscosity activation energy trend.

Such a difference can be related to the different mechanism used in molecule and momentum transport.

In the range of low DMF concentrations the diffusion process corresponds to an actual motion of DMF molecules and a simple rearrangement of water molecules.

However, the DMF molecule's motion requires the breaking and rebuilding of the water hydration shell around each $-CH_3$ group and that of H_2O–DMF hydrogen bonds.

It is reasonable to assume that the barrier to this process increases with increasing DMF concentration.

On the other hand, in the DMF-rich composition range, diffusion corresponds to the motion of H_2O molecules and a rearragement of DMF around them.

Such a motion can be achieved by the simple rotation of a DMF–H_2O couple inside the hole containing them without any extensive participation of the surrounding solvent structure (*24*).

For this reason increasing water concentration promotes a decreasing of diffusion activation energy.

The momentum transport connected with the viscous flow implies a contribution of the bulk of solution so only the maximum is observed, connected with the building of DMF–H_2O extended structures.

Finally we note that unfortunately activity coefficient data are missing and it is impossible to use the Ogston formula (*25*) for the calculation of mobilities.

Registry No. DMF, 68-12-2.

Literature Cited

(1) Guarino, G.; Ortona, O.; Sartorio, R.; Vitagliano, V. *J. Chem. Eng. Data* **1985**, *30*, 366–368.
(2) Kesting, R. E. In "Synthetic Polymeric Membranes"; McGraw Hill: New York, 1971.
(3) Loeb, S.; Sourirajan, S. *Adv. Chem. Ser.* **1962**, *38*, 117–132.
(4) Strathmann, H.; Kock, K. *Desalination* **1977**, *21*, 241–255.
(5) Koenhen, D. N.; Mulder, M. H.; Smolders, C. A. *J. Appl. Polym. Sci.* **1977**, *21*, 199–215.
(6) Sourirajan, S.; Kunst, B. In "Synthetic Membranes"; Sourirajan, S., Ed.; Natl. Res. Council., Canada: Ottawa, 1977; p 129.
(7) Hertz, H. G.; Leiter, H. *Z. Phys. Chem. (Wiesbaden)* **1962**, *133*, 45–67.
(8) Weissberger, A. In "Physical Methods of Chemistry"; Wiley: New York, 1972.
(9) International Critical Tables, Vol. 7, p 13.
(10) Assarson, P.; Eirich, F. R. *J. Phys. Chem.* **1968**, *72*, 2710–2719.
(11) Symons, M. C. R.; Harvey, J. M.; Jackson, S. E. *J. Chem. Soc., Faraday Trans. 1* **1980**, *76*, 256–265.
(12) Oncescu, T.; Jurconi, E. *Rev. Roum. Chim.* **1971**, *16*, 1033–1038.
(13) de Visser, C.; Perron, G.; Desnoyers, J. E.; Heuvelsland, W. J. M.; Somsen, G. *J. Chem. Eng. Data* **1977**, *22*, 74–79.
(14) Saphon, S.; Bittrich, H. J. *Z. Phys. Chem.* **1971**, Bd. 252, H.1/2.
(15) de Visser, C.; Somsen, G. *Z. Phys. Chem. (Wiesbaden)* **1974**, *92*, 159–162.
(16) Dawber, J. G. *J. Chem. Soc., Faraday Trans. 1* **1982**, *78*, 1127–1130.
(17) Assarson, P.; Chen, N. Y.; Eirich, F. R. *Chem. Abstr.* **1975**, *82*, 176109.
(18) Sasaki, Y. et al. *Chem. Abstr.* **1983**, *98*, 153533.
(19) Assarson, P. et al. *Chem. Abstr.* **1969**, *70*, 14825.
(20) Murthy, N.; Manohara, et al. *Chem. Abstr.* **1983**, *99*, 129139.
(21) Rohdewald, P.; Moldner, M. *J. Phys. Chem.* **1973**, *77*, 373–377.
(22) Singh, D.; Bahadur, Lal; Ramanamurti, M. V. *J. Solution Chem.* **1977**, *6*, 703–715.
(23) Stockausen, N.; Utzel, H.; Seitz, E. *Z. Phys. Chem. (Wiesbaden)* **1982**, *133*, 569–577.
(24) Hirtschfelder, J. O.; Curtiss, C. F.; Bird, R. B. In "Molecular Theory of Gases and Liquids"; Wiley: New York, 1954; pp 624–629.
(25) Ogston, A. G. *J. Chem. Soc., Faraday Trans. 1* **1954**, *50*, 1303–1311.

Received for review December 26, 1984. Accepted July 5, 1985. This research was supported by the Italian C.N.R.: Progetti finalizzati—Chimica Fine e Secondaria.

Solubility Products of the Rare-Earth Carbonates

F. Henry Firsching* and Javad Mohammadzadel

School of Sciences, Southern Illinois University, Edwardsville, Illinois 62026

The solubility and the solubility products of 15 rare-earth carbonates in aqueous solution have been determined at 25 ± 1 °C. The most soluble are lanthanum carbonate (pK = 29.91) and erbium carbonate (pK = 28.25) and the least soluble is scandium carbonate (pK = 35.77). Some of the rare-earth carbonates were prepared by precipitation from homogeneous solution with trichloroacetic acid. Saturated solutions were analyzed for pH and the concentrations of rare-earth cation. Activity products were calculated from the experimental data. The solubility of the rare-earth carbonates is so low that the solubility product and activity product are essentially the same value. A thorough search of chemical literature showed only limited information on the solubility of rare-earth compounds in general, and nothing on the solubility of the rare-earth carbonates. Solubility information is essential for general use by scientists. Furthermore, the difference in the solubilities of rare-earth carbonates may provide suitable separation procedures for some lanthanides.

Experimental Section

Preparation of Rare-Earth Carbonates. The rare-earth carbonates can be prepared in major quantities by precipitation from homogeneous solutions with trichloroacetic acid. Decomposition of the rare-earth trichloroacetates in a warm homogeneous solution yields pure crystalline rare-earth carbonates (*1*). Approximately 10 g of rare-earth oxide was dissolved in a slight excess of trichloroacetic acid. The solution was then heated to 90 °C, causing the decomposition of the trichloroacetates. A slight excess of trichloroacetic acid was originally required to dissolve the rare-earth oxide, and the carbonate would not precipitate until the excess acid had been decomposed. Heating was continued for nearly 7 h following the initial formation of the carbonate precipitate. The resulting crystals were washed 10–20 times with deionized water in order to remove any soluble impurities or colloidal material.

Saturated Solutions. The rare-earth carbonates are very insoluble in water. The pure saturated solutions of rare-earth carbonates would contain a rare-earth cation concentration that is on the order of 10^{-7}–10^{-8} M. In order to bring enough

0021-9568/86/1731-0040$01.50/0